Title	Three-dimensional lattice rotation in GaAs nanowire growth on hydrogen-silsesquioxane covered GaAs (001) using molecular beam epitaxy
Author(s)	Tran, Dat Q.; Pham, Huyen T.; Higashimine, Koichi; Oshima, Yoshifumi; Akabori, Masashi
Citation	Physica E: Low-dimensional Systems and Nanostructures, 99: 58-62
Issue Date	2018-02-20
Type	Journal Article
Text version	author
URL	http://hdl.handle.net/10119/16213
Rights	Copyright (C) 2018, Elsevier. Licensed under the Creative Commons Attribution-NonCommercial-NoDerivatives 4.0 International license (CC BY-NC-ND 4.0). [http://creativecommons.org/licenses/by-nc-nd/4.0/] NOTICE: This is the author's version of a work accepted for publication by Elsevier. Dat Q. Tran, Huyen T. Pham, Koichi Higashimine, Yoshifumi Oshima, Masashi Akabori, Physica E: Low-dimensional Systems and Nanostructures, 99, 2018, 58-62, http://dx.doi.org/10.1016/j.physe.2018.01.010
Description	

Three-Dimensional Lattice Rotation in GaAs Nanowire Growth on Hydrogen-Silsesquioxane Covered GaAs (001) Using Molecular Beam Epitaxy

Dat Q. Tran†, Huyen T. Pham, Koichi Higashimine, Yoshifumi Oshima， Masashi Akabori‡

Center for Nano-Materials and Technology, Japan Advanced Institute of Science and Technology (JAIST), 1-1 Asahidai, Nomi, Ishikawa 923-1292, Japan.

Abstract

We report on crystallographic behaviors of inclined GaAs nanowires (NWs) self-crystallized on GaAs (001) substrate. The NWs were grown on hydrogen-silsesquioxane (HSQ) covered substrates using molecular beam epitaxy (MBE). Commonly, the epitaxial growth of GaAs ⟨111⟩B (B-polar) NWs is prominently observed on GaAs (001); however, we yielded a remarkable number of epitaxially grown GaAs ⟨111⟩A (A-polar) NWs in addition to the majorly obtained B-polar NWs. Such NW orientations are always accompanied by a typical inclined angle of 35° from (001) plane. NWs with another inclined angle of 74° were additionally observed and attributed to be ⟨111⟩-oriented, not in direct epitaxial relation with the substrate. Such 74° NWs' existence is related to first-order three-dimensional (3D) lattice rotation taking place at the very beginning of the growth. It turns out that spatially 60° lattice rotation around ⟨111⟩ directions at GaAs seeds is essentially in charge of A- and B-polar 74° NWs. Transmission electron microscope observations reveal a high density of twinning in the B-polar NWs and twin-free characteristic in the A-polar NWs.

Keywords: III-V semiconductors, GaAs nanowires, molecular beam epitaxy growth, vapor liquid solid.

---

†)‡) Correspondence authors. E-mail addresses: dattq@jaist.ac.jp (D. Q. Tran), akabori@jaist.ac.jp (M. Akabori)

I. Introduction

One-dimensional (1D) structures such as nanowires (NWs) have been developed over the last two decades into a large field and they are believed to be building blocks for a wide range of applications. Especially, III-V semiconductor NWs have been intensively studied because they have potential to show high electron mobility and saturate velocity that are important for future high-speed electronic applications [1]. Among them, GaAs NWs have been widely studied so far for nanoelectronic, photonic and photovoltaic applications [2-5]. Up to now, a plenty of work has been done on GaAs NW growth using vapor-liquid-solid (VLS) method in molecular beam epitaxial (MBE) system with the help of metal nanoparticles (NPs) as catalysts [6-8]. Au is the most commonly used catalyst in NW growth using VLS method due to high chemical stability; however, there is a possibility of unintentional incorporation of Au into NWs as impurities forming deep levels, which inherently limit the performance of NW-based devices [9-11]. To avoid such unintentional incorporation of metal catalysts, one of the typical methods is self-catalyzed VLS-MBE using Ga NPs with SiO_2 [12], native oxide [13], or HSQ-based amorphous silicon oxide (SiO_x) [14]. The use of HSQ-based masks shows many advantages compared to the use of usual oxide masks. For instances, uniform nanometer-thick HSQ layers have been achieved by a simple spin-coating method, and the ability of pin-hole self-creation at growth temperature [11]. The self-catalyzed VLS-MBE has been studied mainly on (111)-oriented substrates but less on (001)-oriented ones, which are commonly used in various device applications. Moreover, the growth on GaAs (001) tends to induce a complex NW net [15] due to polar-related or abnormal growth that needs to be systematically investigated.

In this paper, we present the self-catalyzed VLS-MBE growth of GaAs NWs on HSQ-coated GaAs (001) substrates. Through a careful analysis, we show that NWs in optimized conditions are epitaxially grown in not only ⟨111⟩B but also ⟨111⟩A directions, and the inclined angles are estimated to be about 35°. Additionally, NWs slanting 74° from (001) plane are also observed along the same projections with the 35° NWs. A model of first-order three-dimensional lattice rotation is comprehensively discussed to explain the formation of the 74° NWs. Finally, a comparison between ⟨111⟩B and ⟨111⟩A NWs in terms of morphology and crystallography is conducted.

II. Experimental Procedure

After removing native oxides on GaAs surface by an organic-ammonium chemical, the GaAs (001) wafers were spin-coated with an HSQ solution at 5000 rpm in 1 min. The solution consists of Dow Corning Fox 14

and methyl-isobutyl-ketone (MIBK) with the volume ratio of 1:30. Subsequently, the wafers were baked on a hot plate in the air at 150°C in 2 min and then at 300°C in 10 min to transform the spin-coated HSQ layer into SiO_x. The obtained SiO_x thickness was typically 20 nm measured with an ellipsometer. Before loading the substrates into MBE system having three chambers, they were successively cleaned with acetone, methanol, and deionized (DI) water for 5 min in each solution. After loading the substrates, they were heated up and kept at 370°C for 1 hour in transfer chamber for degassing and then transferred to growth chamber. After reaching growth temperature, the substrates were kept in 10 min for thermal stabilization. Subsequently, Ga deposition without opening As shutter was carried out in 20 sec and followed by Ga NP incubation process in 10 min. The NW growth was then started with simultaneously opening both Ga and As shutters. The optimized growth conditions were substrate temperature of 620°C, Ga BEP of 0.04 ML/s, As BEP of 1.3×10^{-6} Torr (V/III ratio of 24), and growth time of 4 hours. After the growth, Ga NP removal procedure was carried out by closing Ga shutter, cooling the sample down to 490°C with keeping As exposure for 1 hour. At the final step, the As flux was continuously kept open during cooling down process.

The NW morphology, density, and inclined angles were analyzed using a scanning electron microscopy (SEM). NWs were transferred onto a copper mesh, and their crystal structure was investigated by means of transmission electron microscopy (TEM).

III. Results and Discussion

Figure 1 shows SEM images of the sample grown in optimized conditions. In Fig. 1a, the top-view image shows two typical types of NWs located on the sample including lower contrast NWs presented by longer lines and higher contrast NWs presented by shorter lines. The NWs of both types point along four orthogonal directions ([1-10], [110], [-110], and [-1-10]). Around NW bottoms, polycrystalline GaAs islands were alternately deposited on SiO_x surface during the growth. From the side views as shown in Figs. 1b and 1c, the NWs incline from (001) plane with two typical angles of 35° and 74°. As a result, the lower and higher contrast NWs observed in Fig. 1a are clarified to be 35° and 74° NWs, respectively. Also, the 74° NWs are marked by the arrows in the top-view image. The NW density of about 0.9 μm^{-2} was achieved that is comparable to the highest value induced from the same growth method on HSQ-covered GaAs(111)B substrates [11]. The lengths and diameters of all NWs are relatively uniform and estimated

to be ~4 µm and ~160 nm, respectively. In addition, they possess the same hexagonal cross section with side facets belonging to {110}. The two typical inclined angles are quantitatively confirmed by the angle distribution plotted based on NWs observed in [110] and [1-10] zones as shown in Fig. 1d. The angle deviation around 35° seems to be smaller than that around 74° in both two zones.

The 35° NWs in [110] and [1-10] zones could be crystallographically indexed to be in ⟨111⟩B and ⟨111⟩A orientations, respectively, based on epitaxial relation with the substrate. In terms of NWs with respect to the inclined angle of 74°, their orientations are indexed nearby ⟨115⟩A/B. If that is the fact, they are impossible to be crystallized into the hexagonal cross section, which is unique for ⟨111⟩ orientations. As commonly observed in B-polar GaAs NWs, twin planes separate the NW into many segments, in which two adjacent ones are mutually associated with a typical 60° rotation around growth axis i.e. ⟨111⟩B [15-17]. And such rotation shall lead to no change in growth direction. If we take 3D lattice rotation on the B-polar NWs into account and set rotation axes to be not only ⟨111⟩B but also ⟨111⟩A, we would observe kinking effect by which the NWs selectively switch to a new direction inclined 74° from (001) plane and observable in both [1-10] and [110] zones. To avoid any confusion in naming ⟨111⟩A and ⟨111⟩B directions attached to the rotation axes, we define them as directions pointing upwards from (001) plane. Different from the already-mentioned 3D rotation on B-polar NWs, our observation showed no kinking effect on 74° NWs. This indicates that the 3D lattice rotation solely takes place at the very beginning of the growth, and we suppose that it occurred on GaAs seeds. The seeds are primary GaAs crystallites epitaxially deposited on substrate. The 3D lattice rotation had been experimentally observed by Uccelli et al. with a growth on non-polar Si(111) substrate [18]. In figure 2, we describe in detail the rotation-based 74° NWs, in which crystal lattice at GaAs seed rotates 60° around both ⟨111⟩A (Fig. 2a) and ⟨111⟩B (Fig. 2b) directions. The rotation around ⟨111⟩A enables possible 74° B-polar NWs having an azimuth of 90° with [1-10]. In contrast to the rotation around ⟨111⟩A, 74° NWs with A polarization could be realized from rotation around ⟨111⟩B resulting in an azimuth of 0° or 180° with [1-10]. From the rotation model, the 74° NWs in [1-10] and [110] zones are classified to be in ⟨111⟩B and ⟨111⟩A orientations, respectively (Fig. 2). It is expected that the 35° A- and B-polar NWs are directly grown on substrate without any lattice change; thereby, they keep epitaxial relation with the substrate. This reflects smaller angle deviation of 35° NWs as already examined (Fig. 1c). Also, the larger angle deviations observed at 74° NWs might originate from an imperfection of the 3D lattice rotation.

In Fig. 3a and 3b, images viewing from top of every single NWs of both A and B-polar types are shown. There exists a tendency that B-polar NWs keep straight from base to top with keeping constant diameters. Distinctly, the diameter is nonuniform on every single A-polar NW, and slightly tapering effect can be seen at the middle part of the wire. The A- and B-polar NWs hold the hexagonal cross section with the side facets of {110} (Fig. 3a and 3b). Nevertheless, there is one nominal distinction being found in the symmetry of the cross section, where 6-fold symmetric one is seen on B-polar NWs and 3-fold symmetric one is observed on A-polar NWs. To approach the 3-fold symmetry characteristic in A-polar NWs, we took into account the difference of angles at six corners of their hexagonal cross section. As a consequence, there are two sets of angle being detected, the first set includes three angles at three corners regarding to <-1-12> directions, together making three-fold symmetry through growth axis. These angles range from 120° to 130° beyond the standard value of 120°, and the average and the deviation are XXX nm and XXX nm, respectively. The second set includes the angles at three remaining corners with respect to <11-2> directions. As opposed to the first set, these angles keep below the standard value and range from 110° to 120°, and the average and the deviation are XXX nm and XXX nm, respectively . This fact demonstrates two different growth rates settled for two different families <-1-12> and <11-2>, in which it is slightly faster in <11-2>. This fact is true for both 35° and 74° A-polar NWs. The self-catalyzed A-polar NWs, in this case, are far different from that synthesized by Wacaser et al. using metal-organic vapor phase epitaxy (MOVPE) with Au catalyst [19, 20]. Literally, the MOVPE A-polar NWs were examined to possess triangular cross section with side facets of {11-2} family [19, 20]. The difference in Miller indices of side facets between the A-polar NWs in the MBE and MOVPE growths might stem from temperature disparity, in which the MOVPE growth was conducted at a temperature less than about 100 °C compared to our MBE growth. It is strongly supported by a B-polar NW growth that the temperature ranges used in the two methods are in agreement to induce distinct side-facet indices, where {110} and {11-2} correspond to the higher and lower temperature ranges, respectively [21]. Additionally, A- and B-polar NWs are solely different at opposite polarity along growth direction, their crystallographic response to growth conditions at sidewalls would, in principle, be similar.

GaAs and other III-V semiconductor NWs are likely to be incorporated by a high density of twinning owing to low energy for the twin formation [22] induced from ionicity in their bonds. However, twinning normal to growth direction mostly locates in B-polar NWs and tends to completely vanish in A-polar NWs

as presented in Fig. 3c-3f that is in accordance with the MOVPE growth [19, 23]. The twins with pure zinc-blende phase in the B-polar wire are specified by a double pattern of selected-area electron diffraction (SAED) as shown in the inset of Fig. 3f. The observed double spot structure in SAED pattern is caused by symmetry in the crystal structure due to twin plane. The growth axis remains normal to (1-11) or (-111) plane that is represented by c spot in the diffraction pattern. Our observation of twinning along <111>B is consistent with twinning usually observed in III-V NWs [23-25]. For the sake of clarifying between spatial twinning causing 3D lattice rotation at GaAs seed as already proposed and twinning normally observed along NWs, it is necessary to clearly separate the growth into two steps. The first step is dominated by the formation of primary seeds, where twinning can spatially occurs in both A- and B-polar directions. The second period is governed by NW growth in a specifically selected orientation. Twinning, in this stage, is restricted by both growth direction and polarity of the NWs, in which twin planes always keep normal to growth direction of B-polar NWs and disappear in A-polar NWs.

It is well known that the GaAs NWs are preferable to B-polar growth, thus GaAs (111)B substrates have been commonly used for vertical GaAs NW synthesis. Indeed, a higher probability for B-polar NWs with 65.9 ± 3.4 % in total was achieved than A-polar NWs with 34.2 ± 5.2 % in total (Fig. 4). Nevertheless, such amount of A-polar NWs located on the sample is remarkable. ⟨111⟩A NWs tend to exhibit much difficulty to be grown even on GaAs (111)A substrate; however, engineering wetting factor at droplet in order to lower A-polar surface energy could strongly enhance ⟨111⟩A NW growth [23]. In VLS method, the growth dynamics is driven by droplet at NW top. In the initial stage, it essentially defines the nucleation of A- or B-polar NWs through which surface energy is preferred. It turns out that the droplet shape with corresponding wetting factor against substrate surface has a mortal impact [23, 27]. Manipulating mask's thickness was examined to be effective for handling wetting factor [27], hence the use of HSQ mask in our growth might contribute to tuning wetting factor close to the favorable condition for A-polar NW growth. A large proportion of NWs undergoes 3D lattice rotation (38.8 ± 5.3 %) as revealed by 74-B and 74-A NWs in Fig. 4. Although the proportion of 74-B is apparently larger than that of the 74-A, it is of importance to note that the occurrence of 3D lattice rotation on each of ⟨111⟩ axes is equivalent.

IV. Conclusion

We investigated VLS-MBE growth of GaAs NWs on HSQ-covered GaAs (001). Both A- and B-polar NWs were discovered and emerged with two typical inclined angles of 35° and 74°. First-order 3D lattice rotation around ⟨111⟩A and ⟨111⟩B directions at GaAs seeds is analyzed to be responsible for the formation of 74° B-polar and 74° A-polar NWs, respectively. Moreover, the occurrence of 3D lattice rotation is equivalent for each of ⟨111⟩ axes. The A-polar NWs were also carefully characterized that they possess twin-free characteristic. This research provides insightful interpretation for the growth behaviors of GaAs ⟨111⟩ NWs commonly obtained on GaAs (001) substrates.

Acknowledgements

References

[1] R. Chau, B. Doyle, S. Datta, J. Kavalieros, K. Zhang, Nat. Mater. **6** (2007) 810-812.

[2] D. Saxena, S. Mokkapati, P. Parkinson, N. Jiang, Q. Gao, H.H. Tan, C. Jagadish, Nat. Photonics **7** (2013) 963-968.

[3] P. Krogstrup, H.I. Jorgensen, M. Heiss, O. Demichel, J.V. Holm, M. Aagesen, J. Nygard, A. Fontcuberta i Morral, Nat. Photonics **7** (2013) 306-310.

[4] X. Miao, K. Chabak, C. Zhang, P. K. Mohseni, D. Walker, X. Li, Nano Lett. **15** (2015) 2780-2786.

[5] M. Yao, N. Huang, S. Cong, C.-Y. Chi, M.A. Seyedi, Y.-T. Lin, Y. Cao, M.L. Povinelli, P.D. Dapkus, C. Zhou, Nano Lett. **14** (2014) 3293-3303.

[6] Z.H. Wu, X.Y. Mei, D. Kim, M. Blumin, H.E. Ruda, Appl. Phys. Lett. **81** (2002) 5177-5179.

[7] J.H. Paek, T. Nishiwaki, M. Yamaguchi, N. Sawaki, Phys. Status Solidi C **5** (2008) 2740-2742.

[8] Z.H. Wu, X. Mei, D. Kim, M. Blumin, H.E. Ruda, J.Q. Liu, K.L. Kavanagh, Appl. Phys. Lett. **83** (2003) 3368-3370.

[9] S. Breuer, C. Pfüller, T. Flissikowski, O. Brandt, H.T. Grahn, L. Geelhaar, H. Riechert, Nano Lett. **11** (2011) 1276-1279.

[10] D.E. Perea, J.E. Allen, S.J. May, B.W. Wessels, D.N. Seidman, L.J. Lauhon, Nano Lett. **6** (2006) 181-185.

[11] M. Bar-Sadan, J. Barthel, H. Shtrikman, L. Houben, Nano Lett. **12** (2012) 2352-2356.

[12] A.F.i. Morral, C. Colombo, G. Abstreiter, J. Arbiol, J.R. Morante, Appl. Phys. Lett. **92** (2008) 063112.

[13] J.H. Paek, T. Nishiwaki, M. Yamaguchi, N. Sawaki, Phys. Status Solidi C **6** (2009) 1436-1440.

[14] T. Rieger, S. Heiderich, S. Lenk, M.I. Lepsa, D. Grützmacher, J. Cryst. Growth **353** (2012) 39-46.

[15] S. Ambrosini, M. Fanetti, V. Grillo, A. Franciosi, S. Rubini, J. Appl. Phys. **109** (2011) 094306.

[16] I. Zardo, S. Conesa-Boj, F. Peiro, J.R. Morante, J. Arbiol, E. Uccelli, G. Abstreiter, A. Fontcuberta i Morral, Phys. Rev. B **80** (2009) 245324.

[17] M. Hjort, S. Lehmann, J. Knutsson, R. Timm, D. Jacobsson, E. Lundgren, K.A. Dick, A. Mikkelsen, Nano Lett. **13** (2013) 4492-4498.

[18] E. Uccelli, J. Arbiol, C. Magen, P. Krogstrup, E. Russo-Averchi, M. Heiss, G. Mugny, F. Morier-Genoud, J. Nygård, J.R. Morante, A. Fontcuberta i Morral, Nano Lett. **11** (2011) 3827-3832.

[19] B.A. Wacaser, K. Deppert, L.S. Karlsson, L. Samuelson, W. Seifert, J. Cryst. Growth **287** (2006) 504-508.

[20] I. Miccoli, P. Prete, F. Marzo, D. Cannoletta, N. Lovergine, Cryst. Res. Technol. **46** (2011) 795-800.

[21] S. Mun Teng, Z. Kun, G. Qiang, T. Hark Hoe, J. Chennupati, Z. Jin, Semicond. Sci. Technol. **31** (2016) 094004.

[22] H. Gottschalk, G. Patzer, H. Alexander, phys. status solidi A **45** (1978) 207-217.

[23] X. Yuan, P. Caroff, J. Wong-Leung, L. Fu, H.H. Tan, C. Jagadish, Adv. Mater. **27** (2015) 6096-6103.

[24] J. Johansson, L.S. Karlsson, C. Patrik T. Svensson, T. Martensson, B.A. Wacaser, K. Deppert, L. Samuelson, W. Seifert, Nat. Mater. **5** (2006) 574-580.

[25] CaroffP, K.A. Dick, JohanssonJ, M.E. Messing, DeppertK, SamuelsonL, Nat. Nanotechnol. **4** (2009) 50-55.

[26] S. Perera, M.A. Fickenscher, H.E. Jackson, L.M. Smith, J.M. Yarrison-Rice, H.J. Joyce, Q. Gao, H.H. Tan, C. Jagadish, X. Zhang, J. Zou, Appl. Phys. Lett. **93** (2008) 053110.

[27] F. Matteini, G. Tütüncüoglu, H. Potts, F. Jabeen, A. Fontcuberta i Morral, Cryst. Growth Des. **15** (2015) 3105-3109.

FIGURE AND CAPTIONS

Figure 1: Scanning electron microscopy (SEM) images taken from (a) top view, (b) side view in [110] zone, (c) side view in [1-10] zone. (d) Distribution of NWs' inclined angles in [110] and [1-10] zones. The angle distribution was calculated from a relatively large number of side-view SEM images at the same magnification and without tilting. The equal numbers of images were taken into account for the two zones [110] and [1-10].

Figure 2: Model of first-order three-dimensional lattice rotation at GaAs seed for the formation of 74° NWs in [1-10] and [110] zones based on spatially 60° rotations around (a) ⟨111⟩A and (b) ⟨111⟩B directions, respectively.

Figure 3: Cross-section SEM images of (a) 35° B-polar and 74° A-polar NWs, (b) 35° A-polar and 74° B-polar NWs. To observe the cross sections of the 35° and 74° NWs, the substrate was tilted 55° and 16°, respectively, with considering substrate crystallographic orientations. (c, d) TEM images of GaAs ⟨111⟩A and GaAs ⟨111⟩B NWs, the corresponding high-resolution TEM images are shown in (e) and (f), respectively. The inset in (f) is selected-area electron diffraction pattern of twin region marked with the white square, where the diffraction spots of two orientations of the twin are observed.

Figure 4: The probability distribution of A-polar and B-polar NWs over the two inclined angles of 35° and 74°. Where 35-B, 74-A, 35-A, and 74-B denote 35° B-polar, 74° A-polar, 35° A-polar, and 74° B-polar NWs, respectively.
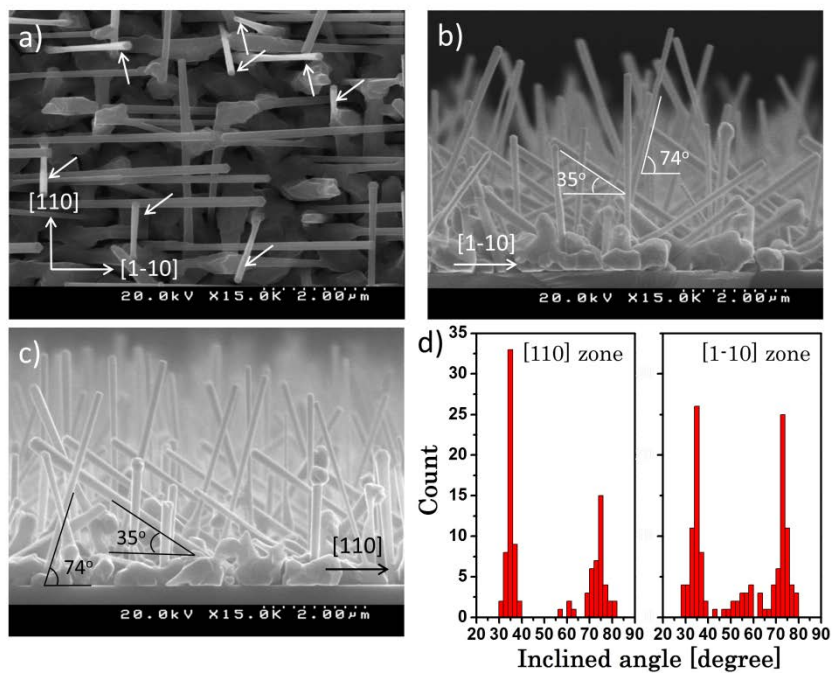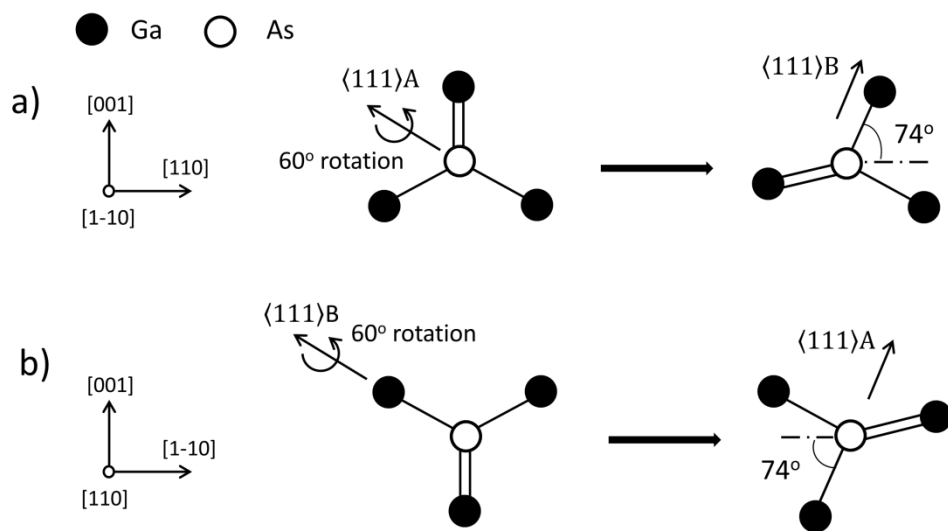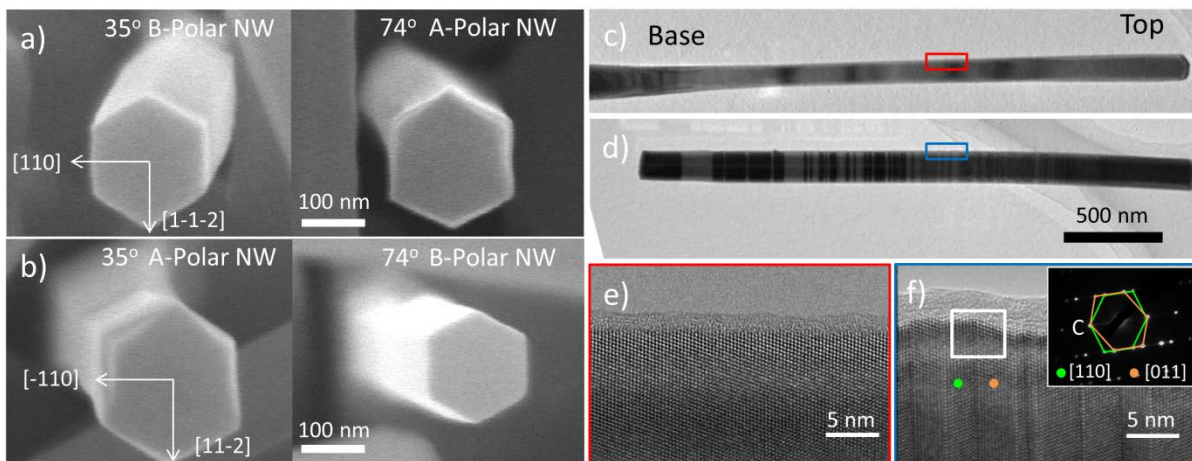
Figure 1

Figure 2

Figure 3

Figure 4